X-ray behaviour of Circinus X-1 - I: X-ray Dips as a diagnostic of periodic behaviour

W.I. Clarkson[1][*][†], P. A. Charles[1], N.Onyett[1,2]

1. School of Physics and Astronomy, Southampton University, SO17 1BJ, UK
2. Astronomy Centre, CPES, University of Sussex, Falmer, Brighton BN1 9QJ, UK

ABSTRACT

We examine the periodic nature of detailed structure (particularly dips) in the RXTE/ASM lightcurve of Circinus X-1. The significant phase wandering of the X-ray maxima suggests their identification with the response on a viscous timescale of the accretion disk to perturbation. We find that the X-ray dips provide a more accurate system clock than the maxima, and thus use these as indicators of the times of periastron passage. We fit a quadratic ephemeris to these dips, and find its predictive power for the X-ray lightcurve to be superior to ephemerides based on the radio flares and the full archival X-ray lightcurve. Under the hypothesis that the dips are tracers of the mass transfer rate from the donor, we use their occurrence rate as a function of orbital phase to explore the (as yet unconstrained) nature of the donor. The high $\dot{P}$ term in the ephemeris provides another piece of evidence that Cir X-1 is in a state of dynamical evolution, and thus is a very young post-supernova system. We further suggest that the radio "synchrotron nebula" immediately surrounding Cir X-1 is in fact the remnant of the event that created the compact object, and discuss briefly the evidence for and against such an interpretation.

Key words: X-rays: binaries, Stars: Individual: Cir X-1, Accretion, Accretion disks, Stars: evolution

1 INTRODUCTION

Cir X-1 is a galactic X-ray binary located in the galactic plane at a distance of 6-8 kpc (Goss & Mebold 1977). Its most well-known feature is strong X-ray variability on a (presumed orbital) cycle of 16.6 days (Kaluzienski et al 1976). The source distance and X-ray lightcurve imply variation of X ray luminosity L_x of a factor $\sim$100 throughout this cycle (e.g. Kaluzienski et al 1976). Radio flares were found at peak levels of 1Jy, on a similar period to the X-ray variations (Haynes et al, 1978), and a similar cycle is evident in the IR activity (Glass 1994). An arcsec-scale asymmetric jet has been imaged (Fender et al, 1998), raising the possibility that outflow from the system is relativistic. During an interval of low X-ray activity, EXOSAT detected eleven X-ray bursts, and their identification with Cir X-1 strongly suggests that the compact object is a neutron star (Tennant et al 1986a,b). Quasi-periodic oscillations (QPO's) have been detected and characterised on two occasions (Tennant 1987,

Shirey et al 1998). The earlier EXOSAT observations suggested Atoll-like behaviour on the X-ray colour-colour diagram, whereas RXTE/PCA observations in the late 1990's show Z-source behaviour (Shirey, Bradt & Levine 1999), implying an external magnetic field strength $\gtrsim 10^9 G$ (van der Klis 1995). X-ray maxima are often preceded by dips in the X-ray lightcurve. Spectral fits with ASCA, RXTE and BeppoSAX during these dips are consistent with a partial covering model, in which the X-ray emision consists of a bright component undergoing varying absorption, plus a fainter component not attenuated by absorbing matter (Brandt et al 1996, Shirey, Levine & Bradt 1999, Iaria et al 2001).

Very little is known about the mass-losing star in this system, due to a high but uncertain amount of extinction to the source. Early classification of this system as an HMXB was based on an optical identification (Whelan et al. 1977) which was later disproven (Moneti 1992) as the single object originally identified was subsequently resolved into three distinct stars. The best optical spectra to date are likely dominated by the accretion disk, with the donor an insignificant component (Johnston, Fender & Wu 1999). The highly uncertain extinction ($5 < A_v < 11$ mag) prevents the IR colours from constraining the nature of the donor (Glass

[*] *Email:* w.i.clarkson@open.ac.uk
[†] *Current Address*: Department of Physics and Astronomy, The Open University, Milton Keynes MK7 6AA, UK

1994). Recent high-resolution IR spectra with IRIS2 on the AAT (Clark et al 2003) show strong hydrogen recombination lines and low-excitation metal lines, which resemble the spectrum of a mid-B supergiant. However the variability of these features makes them entirely consistent also with emission from the accretion disk and/or accretion-driven outflow (note however that A0538-66, a Be binary with a highly eccentric 16.6 day orbit, shows extreme variability in spectral sub-class over its orbital cycle as a result of X-ray irradiation and reprocessing; Charles et al 1983).

Indirect methods of determining the mass of the donor are also indeterminate. Modeling the donor mass and eccentricity from the optical spectra (e.g. Johnston, Fender & Wu 1999) assumes identification of spectral components with the donor, which is clearly uncertain. The apparent radio association of Cir X-1 with the supernova remnant (SNR) G 321.9-0-3 suggested an extremely high transverse velocity of ~ 450 km s^{-1} due to an asymmetric supernova kick (Stewart et al 1993). Subsequent exploration of binary parameter space with this kick velocity as a constraint suggested both an extremely high eccentricity ($0.90 < e < 0.94$) and low donor mass (M_2 likely below 1 $M_\odot$; Tauris et al 1999). However, a recent HST study (Mignani et al 2002) finds no measurable proper motion, implying an upper limit on the transverse space velocity of ~ 200 km s^{-1}. This rules out the association with SNR G 321.9-0-3, thereby leaving M_2 and e undetermined.

The Chandra X-ray Observatory (CXO) detected a remarkable set of strong X-ray P Cygni profiles through periastron passage, corresponding to highly ionised states of Ne, Mg, Si, S and Fe (Brandt & Schulz 2000). The breadth of the lines ($\sim 200 - 1900$ km s^{-1}) and their time variability suggest identification of these lines with highly ionised outflow from the inner region of the accretion disk (Schulz & Brandt 2002). Taken with the radio observations of an expanding jet from the source (Stewart et al 1993, Fender 2003 priv. comm), the emerging picture of Cir X-1 is of an extremely unusual neutron star analogue to the galactic black hole candidate microquasars such as SS433 (see Mirabel & Rodriguez 1999 for a review of stellar jet sources).

The 16.6 day cycle has long been fit with a quadratic ephemeris, based on radio flares measured at HARTRAO between 1978 and 1988 (Stewart et al 1991). This ephemeris shows a comparatively high quadratic correction, which implies a remarkably short characteristic timescale for the period evolution ($P/\dot{P}$) of ~ 5600 years. The longterm X-ray lightcurve of Cir X-1 over the three decades since its identification (Margon et al 1971) was recently examined (Saz Parkinson et al. 2003, hereafter SP03), using Fourier techniques to determine the first ephemeris for this system based on X-ray data alone. Period determination with this method is dominated by the X-ray maxima (section 4), whose large intrinsic phase scatter leads to systematic errors in the resulting ephemeris. Furthermore the average mass transfer rate has clearly varied by factors of at least 10 on a timescale of decades (SP03), the likely effect of which on the binary orbit leads us to doubt the validity of fitting a single ephemeris to all X-ray data based on the maxima alone.

In this paper we examine in detail the RXTE/ASM lightcurve of Cir X-1, and find the periastron X-ray dips provide a superior system clock to the X-ray maxima. Possible explanations for the phase wandering of the X-ray maxima
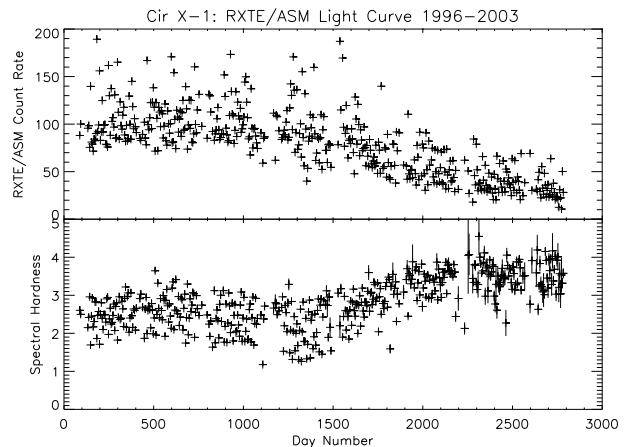

Figure 1. RXTE/ASM dataset used in this paper, binned at 5 days per bin. Throughout the figures in this paper time is shown in units of days elapsed since MJD 50000, i.e. 10th October 1995. **Top:** RXTE/ASM count rate. **Bottom:** RXTE/ASM spectral hardness (see Section 2).

are discussed. We use the resulting measurement of the intrinsic phase profile of the dips to extract information about the orbital eccentricity e and discuss the implication of the X-ray results for the age of Cir X-1 and its future determination. In particular, the high $\dot{P}$ term in the ephemeris suggests the system may be in an early state of post-SN evolution (see also SP03).

2   RXTE/ASM LIGHT CURVE

Launched in December 1995, the Rossi X-Ray Timing Explorer (RXTE) carries an All Sky Monitor (ASM), which gives continuous monitoring of the entire sky (Levine et al 1996, and references therein). Roughly $\sim$10 readings - called "dwells" - are taken of a list of sources per day, lasting about 90 seconds per dwell. Timing information is obtained to within 1/8s, as well as crude spectral information. Data were selected by background and quality of coverage; all points with background level above 10 cs^{-1} were rejected as part of a filtering technnique modeled after Levine et al (2000). The ASM is sensitive to photon energies between 1.3 and 12.1 keV, broken into three energy channels (1.3-3.0 keV, 3.0-5.0 keV and 5.0-12.1 keV). For the purposes of this work, we define the "spectral hardness" as the ratio of activity in the upper two channels to the lower channel, i.e. (3.0-12.1 keV) / (1.3-3.0) keV.

2.1   Methods of analysis

To illustrate the phase variation of features in the lightcurve, and how this can be used as a tool for testing an ephemeris under the hypothesis of steady behaviour, we used the *dynamic lightcurve*. This breaks the dataset into windows of sufficient length to give good statistics, then folds these windows on the ephemeris specified to show the evolution of phase-dependent behaviour as a function of time. One orbital cycle per data window is sufficient to give good signal
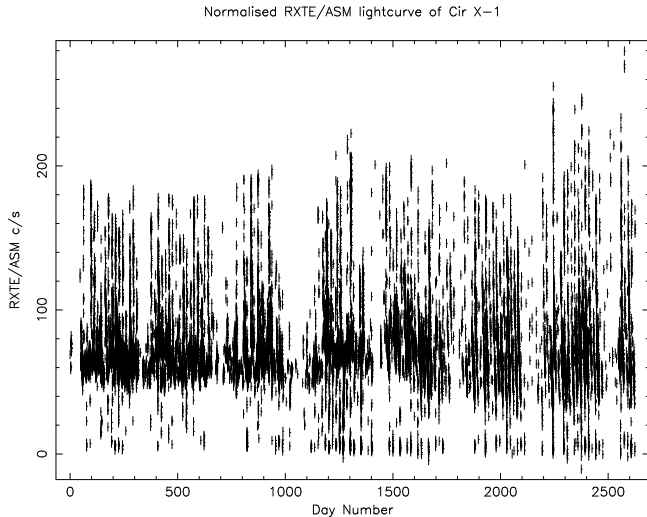
Figure 2. RXTE/ASM lightcurve of Cir X-1, normalised to a running average evaluated over intervals of 200 days (section 3.1). Count rate errors, not overplotted in this figure for clarity, are typically 0.3 cs^{-1} for the "high" state ranging to ~ 3 cs^{-1} for the "low" state.

Figure 3. Distribution in phase of the X-ray maxima, folded on the radio ephemeris (Stewart et al 1991).

to noise to follow the light curve structural changes. Unless otherwise stated, the intensity of the grayscale is directly proportional to the RXTE/ASM count rate.

We examine the usefulness of the pure RXTE/ASM lightcurve for period determination by using a dynamic power spectrum approach (see Clarkson et al 2003a & b for extensive discussion of this technique). The Lomb-Scargle periodogram code (Scargle 1982, 1989) is used in conjunction with a sliding 'data window' to produce power density spectra for a series of overlapping stretches of the time series. Adjustable parameters in the analysis are the length of the data window and the amount of time by which the window is shifted in order to obtain the overlapping stretches of data. The code accounts for variations in the number of datapoints per interval such that the power spectrum resolution is identical for each interval. To ensure the 16.6 day cycle is well sampled we set our window length at 400 days. From suitable Monte Carlo simulations (see e.g. Clarkson et al 2003a) we determine a 3σ accuracy for period determination of ~ 0.01d from sampling alone. However, it should be noted that the orbital period of Cir X-1 is undergoing comparatively rapid evolution, placing a limitation on the appropriateness of Fourier techniques for long datasets.

Beyond Fourier techniques, much of the period determination in this paper is performed under the hypothesis that a certain type of behaviour should (i) be stable over time and (ii) be minimally scattered in phase at the true period. The best-fit ephemeris is then defined as that which minimises the phase scatter of these events over the entire lightcurve. To determine this ephemeris, the start time, period and quadratic correction are varied and for each combination of parameters the resulting phase scatter is determined. The period search was performed over a range of parameters much wider than the variation in ephemerides to avoid bias towards any set of values. The range of values used for the start time MJD_0, period P and quadratic correction, $C \simeq \frac{1}{2}P\dot{P}$, respectively, was ± 5 d, ± 0.2d and
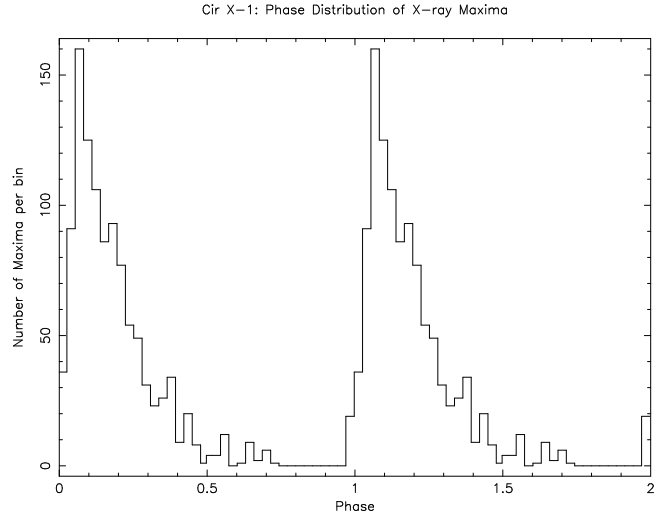
$\pm 10^{-3}$ d. Solutions were then re-examined in finer detail, iterating to the accuracy of the ephemeris determination. When fitting a quadratic ephemeris, at least three orders of magnitude can be saved from the number of computations required by noting that P and C can be determined independently of MJD_0 by subtracting this offset with each fit so that the average phase of the lightcurve features is always zero. Once the optimal combination of P and C has been found, the best value of the offset MJD_0 can then be determined.

3   X-RAY BEHAVIOUR

The X-ray lightcurve can broadly be divided into three separate behaviour types: quasi-regular dips, near phase zero of the radio ephemeris; a "steady" average level beneath which the output rarely drops, except during the dips; and periods of peak activity, during which the output varies erratically from $(1-3)\times$ the steady level. Furthermore, this "steady" level actually evolves in the long-term lightcurve (see Figure 1) and so, for convenience in this paper, we divide the lightcurve into three "states" depending on the steady value. We shall refer to day numbers 0-700 as the "high" state of the source, day numbers 1800-present as the "low" state, and the interval inbetween as the "transitional" region. We urge the reader not to confuse these denominations with the low/hard and high/soft states often used when describing black hole microquasars (e.g. Tanaka & Lewin 1995).

3.1   Longterm Decline

The steady level has decreased dramatically over the 7 years of the RXTE/ASM dataset (Figure 1). During the "high" state this level corresponds to at least 0.7 L$_{Edd}$ for a 1.4 M$_\odot$ neutron star (assuming the lower limit 6 kpc distance), but currently represents perhaps only 0.3 L$_{Edd}$. As pointed out in SP03, the decline represents an apparent return to the X-ray levels of some thirty years previously. This decrease is
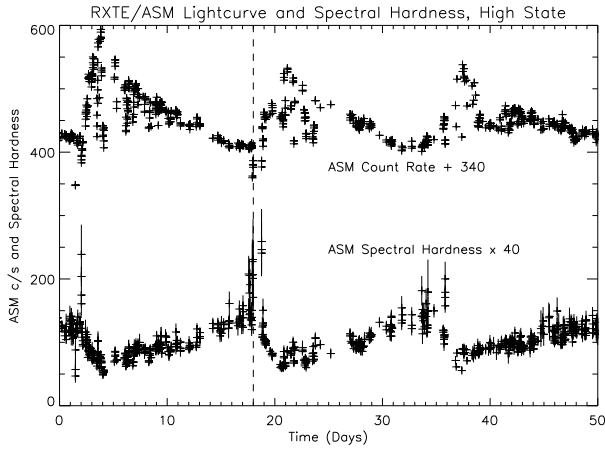
Figure 4. Top: RXTE/ASM spectral hardness for a 50d stretch of the lightcurve starting at day number 490, during the "high" state. Bottom: RXTE/ASM lightcurve during the same state, illustrating the anticorrelation. For one cycle, phase zero according to the radio ephemeris is plotted as a vertical dotted line.
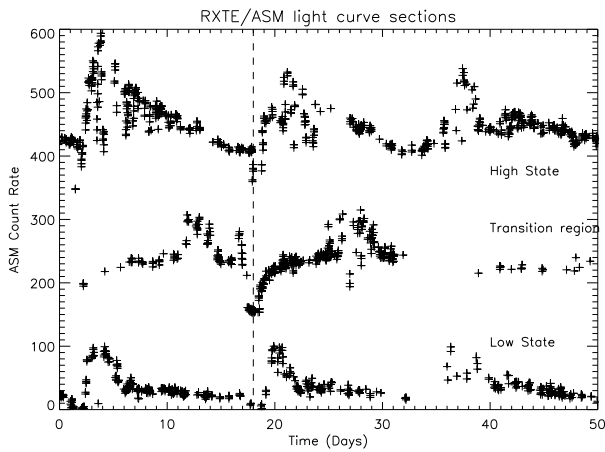

Figure 5. 50-day sections from the RXTE/ASM lightcurve of Cir X-1 corresponding to the three "states" of the lightcurve. Top: starting at day number 490, count rate offset 340 cs^{-1}. Middle: starting day 1425, offset $150cs^{-1}$. Bottom: starting day 2350, no offset. For one cycle, phase zero according to the radio ephemeris is plotted as a vertical dotted line.

accompanied by a corresponding increase in spectral hardness. We attempt to normalise the longterm lightcurve by the "steady" level, by calculating the average count rate over bins of 200 days, boxcar smoothing the result and dividing the instantaneous lightcurve by this running average lightcurve. We notice immediately that to within $\sim 20\%$ the maximum count rate achieved at outburst scales with the running average level (Figure 2).

3.2   X-ray Maxima

The X-ray behaviour at peak activity is extremely erratic and variable, and to some extent appears dependent on the
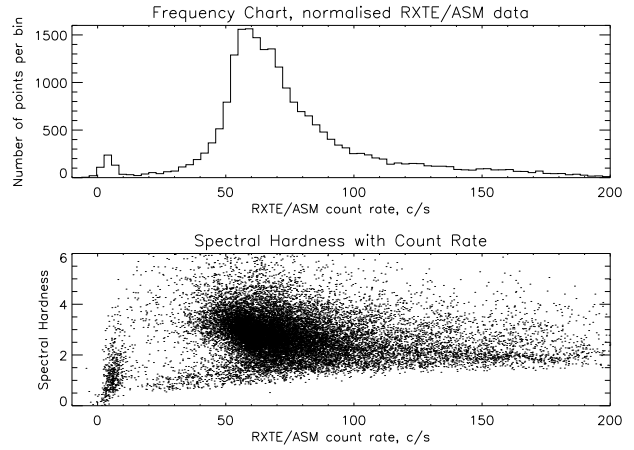

Figure 6. Top: Frequency chart for the entire RXTE/ASM dataset indicates the existence of a separate population of low-count rate "dips." Bottom: ASM hardness-count rate plot for the RXTE/ASM dataset.

source state. During the "high" state the X-ray output varies erratically between the steady level and an envelope described by the histogram in Figure 3. Also present during a few cycles is a smaller secondary maximum, which appears to be similar to a secondary maximum in the radio light curve during this state (Fender 1998). During the "high" state the spectral hardness is anticorrelated with the X-ray activity (see Figure 4). The "transitional" interval shows similar evolution of the spectral hardness to the "high" state. The X-ray maxima do not appear to be accurate system clocks, as they occur across a large range of phases in the 16.6 day cycle (Figure 5 and section 4). Furthermore, the shifting during this interval of the occurrence of the maxima to phase 0.5 and later has uncovered an apparent gradual recovery in X-ray output from a low level at phase zero (Figure 5, middle). The lightcurve during the "low" state appears less erratic than the previous two states, with fewer maxima and less phase wandering (Figure 5, bottom).

3.3   X-ray Dips

Phase zero in the radio ephemeris approximately predicts the quasi-regular dips in X-ray intensity (Shirey 1998). These dips form a separate population of datapoints, as can be seen from the frequency-count rate chart of the ASM dataset (Figure 6). When folded on the radio ephemeris, we see that the dips show far less scatter about phase zero than do the maxima (Figures 7 & 8). X-ray dip spectra are best fit with a two-component model, with a strongly absorbed bright component and an unabsorbed faint component (Section 1). Similar behaviour is seen during X-ray dips in RXTE/PCA observations of black hole candidates GRO J1655-40 and 4U1630-47 (Kuulkers et al 1998).

4   EPHEMERIDES

As the best X-ray system clocks, the dips can be used to test the various published expressions for the ephemerides of Cir X-1. Until very recently, the most commonly used was the
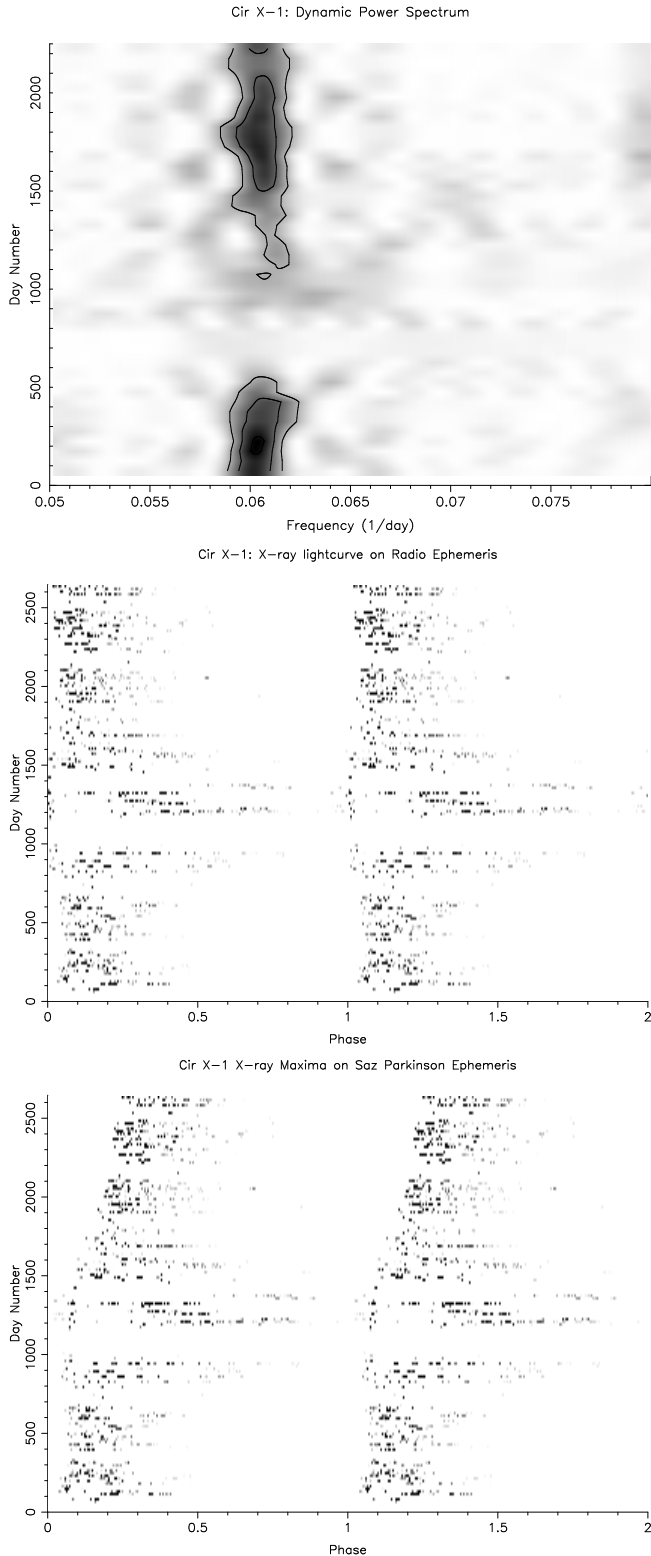
Cir X-1: Dynamic Power Spectrum

Cir X-1: X-ray lightcurve on Radio Ephemeris

Cir X-1 X-ray Maxima on Saz Parkinson Ephemeris

Figure 7. *Top:* Dynamic Power spectrum of the full RXTE/ASM dataset. *Middle:* Dynamic Lightcurve showing the X-ray maxima, folded on the radio ephemeris. *Bottom:* Dynamic lightcurve showing X-ray maxima, folded on the SP03 ephemeris. Note that for the dynamic power spectrum the day numbers represent the beginning of each 400-day data window in the power spectrum.

radio ephemeris (Stewart et al 1991), which, when extrapolated to January 1996 (the beginning of the RXTE/ASM dataset) can be expressed as (Shirey 1998)

$$MJD_N = 50082.04 + (16.54694 - 3.53 \times 10^{-5}N)N \qquad (1)$$

where N is the cycle number. This ephemeris shows an r.m.s. scatter of 0.06 days (Section 1 and Stewart et al 1991), or a 3σ scatter in flare occurence of ~ 0.36 days when extrapolated to the beginning of the RXTE era. As this ephemeris is based on radio data now more than 15 years old, its deteriorating predictive power makes an updated ephemeris desirable. The recent FFT-based analysis of all long-term X-ray datasets of Cir X-1 (SP03) provided the first ephemeris based on X-ray activity alone. This ephemeris retains MJD_0 from the radio ephemeris, but other than this constant offset the two are independent. When precessed to the beginning of the RXTE/ASM dataset, this X-ray ephemeris is expressed as:

$$MJD_N = 50082.04 + (16.5389 - 1.354 \times 10^{-4}N)N \qquad (2)$$

with 3σ errors on the period P and quadratic correction C of $\sim 1.7 \times 10^{-2}$d and $\sim 1.39 \times 10^{-6}$d respectively.

We test the suitability of the x-ray maxima for period determination by plotting the dynamic power spectrum of the entire RXTE/ASM lightcurve of Cir X-1 with the dynamic lightcurve (Figure 7). Error in the period determinations is manifested as a systematic drift in phase from cycle to cycle. The transitional period, during which the maxima wander considerably in phase, corresponds to the interval noted by SP03, during which the 16.6d cycle is suppressed. This suggests that the outbursts dominate the period detection from such methods, which is why the transitional region was excised from the RXTE/ASM lightcurve by SP03 when determining their ephemeris.

The radio ephemeris (Figures 7 & 8) shows less of a drift, particularly in the dynamic lightcurve of the X-ray maxima, but a systematic drift in the occurrence of the dips is still visible from day number 1000 onwards. The extrapolated scatter in the radio ephemeris (section 4) leads to 3σ phase error of $\sim \pm 0.025$ by the end of the RXTE dataset, but this is still small compared to the systematic shift in phase of ~ 0.1 that we observe. Consequently, we do not believe that this shift can be explained by the extrapolated uncertainty in the radio ephemeris alone. The radio ephemeris is currently quite accurate in predicting the onset of dip events, but is expected to become less accurate as the events drift farther backwards in phase.

4.1 Ephemeris based on X-ray Dips

When folded on the radio ephemeris, we see that the dips show far less scatter about phase zero than do the maxima (Figures 7 & 8). Based on the hypothesis that the dips near phase zero on the radio ephemeris are in some way related to the binary orbit, and thus should provide a good system clock, we have attempted to fit an ephemeris on the X-ray dips alone (as described in section 2.1). The radio flares to some extent correlate with the X-ray dips (Shirey 1998), suggesting a causal link, but at present little is known about the mechanisms producing either the radio flares or X-ray dips, which makes it impossible to exploit their relative timing. We minimise assumptions by keeping the time of phase
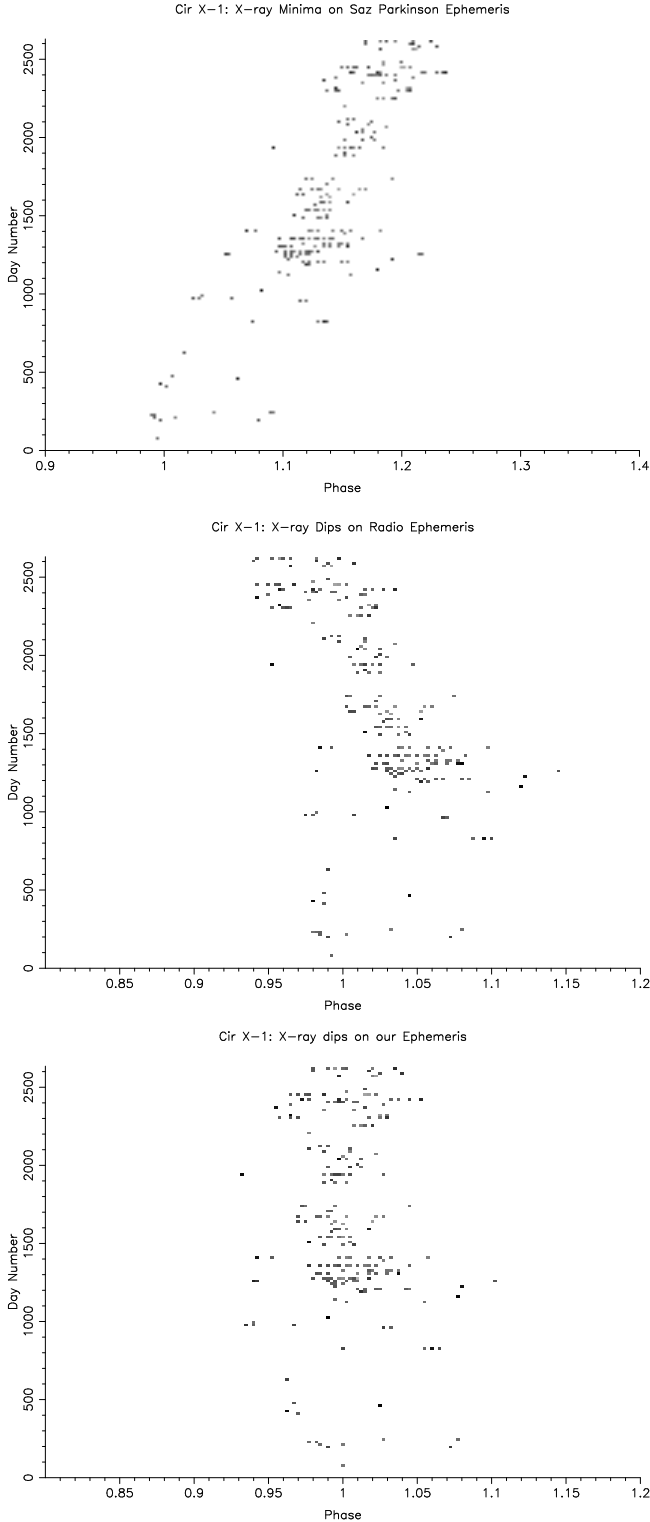
Figure 8. *Top:* Dynamic lightcurve of X-ray Dips, folded on the SP03 ephemeris. *Middle:* X-ray dips folded on the radio ephemeris. *Bottom:* X-ray dips folded on our ephemeris. In this figure the grayscale is inversely proportional to the RXTE/ASM count rate.
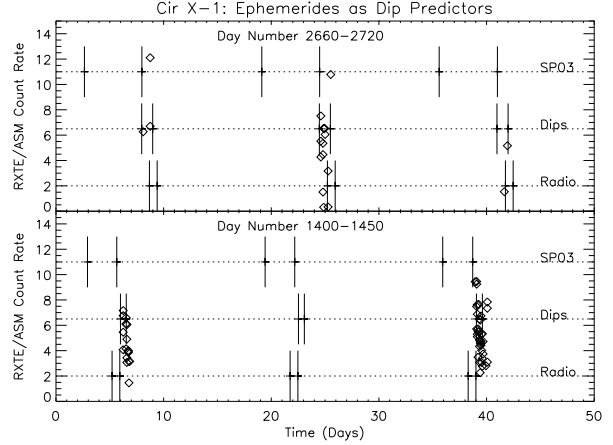

Figure 9. RXTE/ASM lightcurve at two epochs (diamonds), with 3σ bounds on the timing of X-ray dips, as predicted by the three ephemerides (section 4). In each plot the ephemerides, from top to bottom, are based on the X-ray maxima (SP03), X-ray dips (this work) and radio flares (Stewart et al 1991). Ephemeris predictions offset for clarity; no prediction of count rate during dipping is made.

zero as a free parameter in the fit. (If instead the best fit ephemeris is calculated holding MJD_0 at the same value as the radio ephemeris, the smallest value of the phase scatter with respect to phase zero is increased by about 15%). The result of dip phase minimisation is the following ephemeris:

$$MJD_N = 50081.76 + (16.5732 - 2.15 \times 10^{-4}N)N \qquad (3)$$

with 3σ errors on the ephemeris components MJD_0, P and C of 8.7×10^{-2}d, 3.2×10^{-3}d and 2.6×10^{-5}d respectively (section 2.1).

We test the predictive power of this X-ray dip ephemeris by plotting the occurrence of dips against its predictions. As can be seen in Figures 8 & 9 , the dip ephemeris predicts the occurrence of dips with a higher degree of accuracy than the radio or bulk X-ray ephemerides. In broad agreement with the SP03 ephemeris, we find a quadratic correction term almost an order of magnitude above that suggested from the radio ephemeris. It appears that MJD_0 for the X-ray dips occurs approximately 7 hours *earlier* than for the radio flares, but this lag is within the extrapolated error of the radio ephemeris of $\sim$0.36 days (8.5 hours).

5   DISCUSSION

The central issue with Cir X-1 has been the nature of the companion star, and the ASM lightcurve does not appear immediately to resolve the issue. Furthermore, the system eccentricity and inclination have not been constrained (we note that the eccentricity is also only estimated for A0538-66, the prototypical Be XRB, whose X-ray lightcurve, when active, is strikingly similar to Cir X-1; Charles et al 1983). We examine here the use to which the RXTE/ASM lightcurve can be put to address these issues.

5.1   The X-ray maxima

The significant phase wandering of the maxima during the "transitional" state of the lightcurve suggests that they are associated with some feature of the system that is not entirely locked into the orbital clock. This feature is not completely independent of the orbital clock either, as there are still *no* cycles for which an X-ray peak appears between orbital phase 0.8 and 0.9, although during the "transitional" interval there are cycles in which the peak occurs slightly *before* phase zero. The X-ray dips appear to be a better system clock than the outbursts, and we identify their occurrence with changing mass transfer from the donor during periastron passage (sections 4.1 & 5.2). Stellar wind accretion cannot account for the phase wandering of the maxima; for example, in the case of GX301-2, an eccentric ($e = 0.462$) X-ray binary in which the accretion takes place via wind plus a small accretion stream (Leahy 2002), the phase wandering of maxima is tiny compared to that for Cir X-1. We are thus left with the accretion disk to provide the source of material for the maxima, as it is capable of doing so in a manner that could show sufficient variation in the time of occurrence.

The mechanism to do so is not immediately clear. The obvious analogy would be the dwarf nova cycles seen in cataclysmic variables (Warner 1995), however this interpretation suffers obvious limitations. The irradiation from the neutron star is likely to keep the inner disk in a permanent high state, suggesting such cycles would require extremely fine tuning (e.g. Frank, King & Raine 2002). Furthermore, this model does not account for the scaling of the X-ray output at maximum with the light curve mean (see section 3.1).

We prefer to argue that the X-ray maxima are due intervals of increased mass transfer onto the compact object as a result of a combination of disk perturbations and varying mass transfer rate, both driven to some extent by the eccentric orbit. These variations will occur at or near the viscous timescale of the disk as this is the timescale for disturbances to propagate through the disk. This interpretation has the attraction that it allows the outbursts to occur over a quasi-steady base level of accretion, as is observed with RXTE/ASM: such response to perturbations will occur preferentially in the outer disk, where material is closer to the impact region of the varying mass transfer stream. This model also has the benefit of predicting how the amplitude of the maxima will vary with the running average: both should scale with the global density of matter in the accretion disk.

It is still unclear what causes the phase of the X-ray maxima to vary so wildly during the "transitional" region, but this interval does immediately precede the longterm return to low levels of X-ray output, so therefore may be related to it. However, it is also possible that the longterm decline is part of an even longer-term pattern of variation in the mass transfer from the donor, possibly due to tidal evolution of the system (see section 5.5).

An alternative model for both the longterm variation outburst level and the phase wandering thus involves Cir X-1 as a Be/X-ray transient, in which the reformation and destruction of the equatorial disk provides the mechanism for the variation of the X-ray lightcurve on a timescale of decades. Variations in the phase of X-ray maxima on

a timescale of years are then produced by the precession of the equatorial disk and/or evolution of 2D structure in this disk. It is known that in several Be/X-ray transients with similar orbital periods to Cir X-1, the equatorial disk is tilted with respect to the plane of the orbit and precesses (e.g. V0332+53; Negueruela et al 1999, 4U 0115+63/V635 Cas; Negueruela et al 2001, hereafter N01). This disk may also be destroyed and reformed on a timescale of months - years, as seen in V635 Cas (N01). Furthermore, 2D structure in equatorial decretion disks through global one-armed oscillations is predicted theoretically (Okazaki 2001) and indeed suggested observationally from V/R variability in several Be/X-ray transients on a timescale of years to decades (Hanuschik et al 1995). The high and unknown reddening towards Cir X-1 makes constraining such models extremely difficult for the forseeable future (c.f. Clark et al 2003).

5.2   X-ray dips as tracers of $\dot{M}(t)$

Using the X-ray dip ephemeris, the dip occurrence rate depends strongly on orbital phase, as all dips are clustered around $\pm \sim 1$ day of phase zero. That this is in sharp contrast to the maxima used by SP03 to determine the ephemeris does not invalidate their discussion, as we are examining a different feature of the lightcurve. We examine here the information that can be extracted about the binary components from this property.

Absorption dips have been used as a diagnostic in the RXTE/ASM lightcurve of the near-circular orbit black hole candidate Cyg X-1 (Balucinska-Church et al 2000). In this case the occurence rate of X-ray dips was also shown to vary strongly with orbital phase, in a manner dependent on the line of sight to the binary: the dips occured with greatest frequency when the donor passed directly in front of the accretor. In this model the X-ray dips are due to photoionisation in the wind of the donor. In the case of Cir X-1, however, the near-coincidence of the dips with times of maximum activity at other wavelengths (and thus periastron passage) suggests the semimajor axis of the binary orbit would have to be almost aligned with our line of sight to the binary, which we reject as requiring fine tuning.

However, subsequent studies of Cyg X-1 with RXTE/PCA divide the X-ray dips in Cyg X-1 into two populations based on spectral behaviour: "Type A" dips, concentrated about donor interposition phases as above, and "Type B," which occur throughout the orbit (Feng & Cui 2002). One suggestion put forward for these dips is absorption of an X-ray emitting region by optically thick "clouds" in the accretion flow near the accretion disk. The number density of such clouds in the vicinity of accretion stream impact in the outer disk scales strongly with $\dot{M}$ (equation 10 of Frank, King & Lasota 1987, hereafter FKL87). In an eccentric system such as Cir X-1, $\dot{M}$ will be a strong function of orbital phase (see Charles et al 1983 or Brown & Boyle 1984). We thus identify the X-ray dips exhibited by Cir X-1 as "Type B" dips, which here occur only during episodes of enhanced mass transfer at periastron passage. This has the attraction of removing the need for fine-tuning of the line of sight to the system.

The accretion disk will respond to changes in $\dot{M}$ on its viscous timescale. We can estimate this value from the phase spread in the outbursts (Figure 7 and section 5.1)

or alternatively from assumptions on the mass transfer rate and viscosity (Frank, King & Raine 2002), to be of order 10 days. The inner disk can respond more quickly but is likely to be highly ionised (Brandt & Schulz 2000), thus will not figure in the formation of the X-ray dips. The response of the accretion disk to varying $\dot{M}$ thus occurs on too long a timescale to affect the relationship between $\dot{M}(t)$ and the occurrence rate of the dips.

The velocity of the gas flow in the accretion stream will be greater than the adiabatic or isothermal sound speeds, allowing internal shocks to be neglected in the direction of the flow (c.f. Frank, King & Raine 2002; we assume further that any variation in sound speed along the stream due to changing $\dot{M}$ is insufficient to bring the sound speed above the freefall velocity at any point in the stream). The sound travel time across the stream will be long compared to the transfer time to the accretion disk (c.f. Lubow & Shu 1975), so we neglect the internal response of the gas in the accretion stream. The impact of the accretion stream on the disk results in shock formation and the condensation of cold absorbing clouds on a timescale similar to the recombination timescale t_{rec} (FKL87), $\sim$ 1-30 minutes for the parameters of Cir X-1. The evaporation timescale for such clouds is of order a few dynamical timescales t_{dyn} (FKL87, Krolik, McKee & Tarter 1981), so they will persist for $\gtrsim$5 hours. The formation rate of clouds leading to X-ray dips will thus respond quickly to changes in $\dot{M}$, and furthermore such dips will persist for a long enough interval to affect the X-ray lightcurve. The $\gtrsim$ 5 hour timescale for cloud evaporation suggests reduction in dip occurrence rate may lag shortly behind the reduction in $\dot{M}$, which is fully consistent with the slight apparent asymmetry in the dip population (Figures 8 & 10).

5.3 Using the dips to investigate the binary parameters

We attempt in this section to relate the rate of occurrence of X-ray dips to the donor mass M_2, the eccentricity e and the donor temperature T. To do so we require a model predicting $\dot{M}(t)$ as a function of these parameters. A preliminary theoretical investigation of $\dot{M}(t)$ due to tidal lobe overflow in an eccentric-orbit binary was undertaken by Brown & Boyle (1984; hereafter BB84). They model the mass transfer as as overflow across an instantaneous tidal lobe (analogous to the Roche Lobe in the circular case), with the constraint added that matter must move with positive velocity relative to the instantaneous tidal lobe, for accretion to occur. This estimates the effect of the changing size of the tidal lobe throughout the binary orbit. This correction also has the effect of shifting the peak in $\dot{M}$ slightly earlier than true periastron. This semianalytic approach was followed up by numerical simulation (Boyle & Walker 1986), exploring the range of parameter space for which capture of transferred matter might occur, in an attempt to model the X-ray activity of A0538-66. Only a single binary orbit was followed in these simulations, so it is not possible to determine the fate of material not immediately captured by the neutron star. Earlier simulations (Haynes, Lerche & Wright 1980) did not take into account hydrodynamic effects, but in covering more orbits suggested that matter not immediately accreted in one periastron passage may be accreted in sub-

sequent cycles, complicating the accretion profile. We thus reject the capture condition espoused by Boyle & Walker (1986), in which gas is only captured if its specific potential energy is greater in magnitude than its specific kinetic energy. More modern simulations of eccentric orbit accreting systems suggest this subsequent accretion may be extremely important in determining the X-ray output of an eccentric binary (Podsiadlowski 2003 priv. comm.). However, as our interest is not in the X-ray generation rate per se but in absorption due to the matter stream, we take the BB84 model for lack of current alternatives. The reader is therefore cautioned that the model on which our constraints will be based is in some sense a preliminary one.

5.4 A simple model

We attempt to fit the profile of dip occurrence rate as a function of M_2 and e. The major source of uncertainty in the BB84 model is the exponential dependence of $\dot{M}(t)$ on the factor

$$\beta = \frac{a(1-e)}{H_p} \qquad (4)$$

where H_p is the (as yet unknown) pressure scale height at the surface of the donor at periastron passage ($H = kT/m_p g$) and a the semimajor axis of the orbit. We make the assumption here that the donor fills its tidal lobe at periastron, allowing us to use the Roche Lobe prescription (Eggleton 1983) for the radius of the donor. The known orbital period thus allows us to place the following constraint on the factor β:

$$\beta \simeq 106 \left(\frac{q}{f^2(q)(1+q)^{1/3}} \right) \left(\frac{1}{T_4(1-e)} \right) \qquad (5)$$

where $f(q)$ is the tidal lobe radius at periastron as a fraction of the semimajor axis (Eggleton 1983), $q = M_2/M_1$ and T_4 is the temperature at the surface of the donor, at periastron, in units of 10^4 K. As the X-ray dips occur over a very limited phase range, we neglect any radius variation that may occur in the donor over the course of the periastron passage, beyond the variation of the tidal lobe itself. Furthermore, we follow Charles et al (1983) in assuming the surface of the donor corotates with the orbit. It is currently unclear what the quantitative effect of non-synchronous donor rotation will be on the $\dot{M}(t)$ profile. We expect the change in the amount of matter ejected from the surface of the donor to compete with an opposing change in the amount of matter that can be captured by the accretor (e.g. Petterson 1978), however the balance of the effects is far from obvious. In the absence of a model for the phase dependence of this behaviour, we retain the assumption of corotation. We merely caution here that if Cir X-1 is a dynamically young system, as suggested by its apparent eccentricity and other behaviours (section 5.5), non-synchronous rotation is a distinct possibility.

We plot the dip occurrence profile, along with an example $\dot{M}(t)$ prediction, in Figure 10. As can be seen, the profile can be fit quite readily with the tidal lobe model, within the errors (assumed gaussian) between the measured X-ray dip rate and the intrinsic cloud formation rate (section 5.2). For the following analysis, dips occurring in the phase range (0.95 - 1.05) are used, as outside this region the
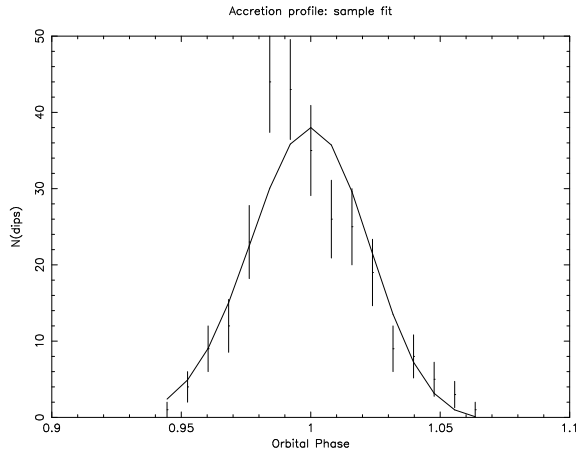
Figure 10. X-ray dip occurrence profile as a function of (presumed orbital) phase. Overplotted is a sample prediction of the BB84 model, in this case M_2=2, e=0.4, H_p=7.5 × 10^4 km.

Figure 11. Combinations of orbital eccentricity and donor mass that fit the observed dip occurrence rate profile. From left: T_4=0.1, 0.5, 1.0, 5.0, 10.0, 50.0 and 100.0 respectively.

errors are comparable to the observed dip rate. Clearly the fit is degenerate, in that in principle any combination of q, T_4 and e can reproduce the observed dip profile. We narrow the parameter space somewhat by noting that the donor mass is unlikely to exceed the $\sim 15 M_\odot$ necessary to form a neutron star (Tauris & van den Heuvel 2003) or else it would have noticeably evolved. More stringent constraints on the donor mass through direct detection of the sytem are not possible due to the uncertain location of the IR-emitting regions (Clark et al 2003) and the uncertain level of reddening (Glass 1994).

A large range of T_4 is in principle possible, as there are several sources of energy dissipation that could heat the surface of the donor significantly above its unperturbed value of $T_4 \sim 0.5 - 1$. The accretor has been among the brightest X-ray sources in the sky, so might be expected to irradiate the donor to $T_4 \gtrsim 10$ (e.g. van Teeseling & King 1998; we neglect here the enhanced mass loss such a mechanism might produce). The supernova itself may have deposited a large amount of energy in the donor leading to significant heating of the stellar envelope to $T_4 \sim 10$ (Marietta et al 2000, Podsiadlowski 2003). Finally, if the system really is eccentric, tidal circularisation will give rise to internal heating of the donor, also bringing T_4 to ~ 10 or higher (see Podsiadlowski 1996). To account for these possibilities, we repeat the $\dot{M}(t)$ profiles for several input values of T_4 in the range ($0.1 \leqslant T_4 \leqslant 100$). For each combination of parameters, the least-squares fit to the dip profile is evaluated and the parameters that fit the profile most closely retained.

The results are plotted in Figure 11. We note that the condition of tidal lobe overflow at periastron leads to larger scale heights than is usually the case ($\sim 10^4$ km), though still small compared to the stellar radius. The reader is urged to bear in mind that the low number of dips recorded per bin by RXTE/ASM leads to significant uncertainty in the true dip occurrence profile (Figure 10). Monte Carlo simulations suggest that the values of $M_2(e)$ calculated from fitting these dips are thus uncertain to a 3σ error of at least 50%. Above $T_4 \sim 5$ the factor β becomes largely insensitive to the donor mass M_2, and *all* combinations occur at $e \gtrsim 0.6$. We note further that the values of $M_2(e)$ should be considered
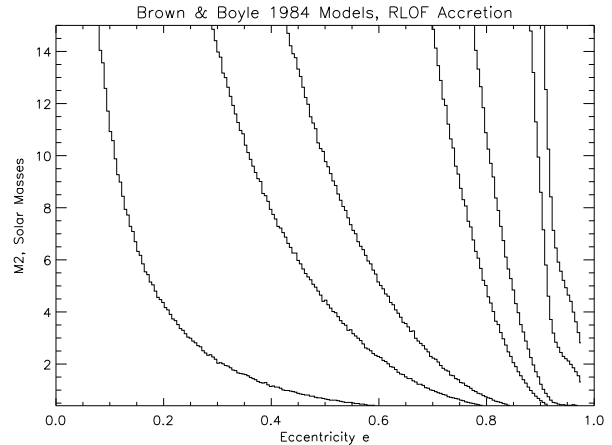
lower limits, as the true $\dot{M}$ profile may be narrower than the X-ray dip occurrence profile (see section 5.2), which would shift the curves upwards in M_2. We thus make no attempt to determine the value of M_2 from our simulations, opting instead to determine regions of e for which solutions exist for reasonable values of T_4.

As expected, for the same width of $\dot{M}$ profile, larger eccentricities correspond to lower values of M_2 and thus lower donor radius. Perhaps surprisingly, low eccentricities are not in principle ruled out, although they do require both low surface temperatures and large donor masses. However, the surface of the donor is likely to be significantly heated by any mechanisms discussed above (so $T_4 \gtrsim 5$). Thus, within the limitations of the model (see above), the system is likely to be at high eccentricity ($0.6 \lesssim e \lesssim 0.95$) for all M_2 (Figure 11). More accurate limits await the results of more detailed simulations of $\dot{M}(t)$ for highly eccentric x-ray binaries.

5.5   Is Cir X-1 a very young system?

The results from the above toy model suggest the system must be in a state of high eccentricity, leading to a natural interpretation with Cir X-1 in an early stage of post-supernova evolution. We urge the reader to bear in mind the limitations of the above model, however; in particular the assumption of corotation will likely not hold for a young system. In the case of a non-irradiated donor with a thick convective envelope, the synchronisation timescale can be estimated at $\gtrsim 10^6$ years for a 16-6 day orbit (Zahn 1977), suggesting the effects of nonsynchronous donor rotation should be considered before general limits can be placed on the binary orbit. In particular the balance between the competing effects of non-synchronous rotation will likely depend on orbital phase. Without a robust exploration of the effect of non-synchronous donor rotation on the accretion profile it is impossible to place limits on the discrepancy between our simulations and the true accretion profile. Our limits on the eccentricity thus apply only to the special case in which corotation has been achieved but circularisation has not. If the system were much older than $\sim 10^6$ years, this case might apply: the synchronisation timescale for a 16.6-day orbit is

a factor $\sim 10^{2-4}$ longer than the circularisation timescale for the range of q used in the above model (Zahn 1977).

The ephemeris based on the X-ray dips is a stronger indicator of the age of Cir X-1. The X-ray dip ephemeris establishes a characteristic timescale $P/2\dot{P}$ even shorter than that suggested by the SP03 analysis, at $\sim$1000 years. If the system were in a state of tidal evolution shortly after the supernova, the system components may not yet have achieved corotation and alignment of their spin axes. The evolution to alignment is expected to give rise to high amplitude variations in mass transfer on a timescale of decades or more (Podsiadlowski 2003, priv. comm.). A look at the long-term X-ray history of Cir X-1 (e.g SP03) shows variability by a factor of at least 10 on such a timescale. This may be further evidence that the system is evolving dynamically, though without ruling out other explanations for such long-term apparent variation, no definite claim can be made.

However, Cir X-1 is surrounded by a synchrotron radio nebula approximately 5×10 arcmin^2 (Stewart et al 1993). Now that the association with SNR G321.9-0.3 has been ruled out (Mignani et al 2002), we propose that this radio nebula may in fact be the supernova remnant of Cir X-1. (When completing this paper we became aware (Fender 2003, priv. comm.) of others exploring this possibility, but believe it has not yet been discussed in the literature.) Such a conclusion is consistent with standard SNR expansion models, and the high reddening would obscure optical emission from the nebula. With a diameter of ~ 8 pc, the remnant would likely be in the Sedov-Taylor stage, which implies $\gtrsim$ 4,000 years have elapsed since the supernova (e.g. Choudhuri 1998). Comparison with observed SNRs at this stage of evolution (e.g. Hughes, Hayashi & Koyama 1998) suggest the X-ray luminosity is likely to be $L_X \sim 1 - 50 \times 10^{35}$ erg s^{-1}, or roughly 1% the "steady" output of the point source. A study of archival XMM and Chandra observations of Cir X-1 (Clarkson & Charles 2003) shows that, in the region occupied by the radio nebula, X-ray emission is dominated by ISM scattering of the bright central point source. This scattered component is bright enough to mask any X-ray SNR at the location of Cir X-1, allowing no direct determination of the existence or otherwise of an X-ray counterpart to the nebula. The light travel time of reflected paths is long enough to cause pessimism of the chances of sucess of a search for a SNR during intervals of dipping.

5.6   The External Magnetic Field of the Neutron Star

The primary objection to the young source scenario has always been that the external magnetic field of the neutron star is observed to be much weaker than expected for a young system, as suggested by the existence of Type I bursts (Tennant et al 1987) and Z-source QPOs (Shirey, Bradt & Levine 1999), and the repeated non-detection of X-ray pulsations (though the latter is inclination-dependent). We suggest the discrepancy may be resolved by accretion-induced screening of the core magnetic field. Detailed consideration of the accretion and screening process is beyond the scope of this work: we merely summarise the model and recent results. Matter initially channeled onto the magnetic poles spreads under the weight of the accretion column to cover the surface of the neutron star. This matter is a fully ionised

plasma, and therefore is diamagnetic, leading to the screening of the internal magnetic field (Taam & van den Heuvel 1986: see Choudhuri & Konar 2002 for a review). Advection of the screening layer then submerges the internal magnetic field (Romani 1990). Evolution of the external field then depends on the competition between the timescales for advection of the accreted matter and for ohmic diffusion of the internal field into the newly accreted matter (Konar & Bhattacharya 1997). The internal field will break through the screening on the timescale for ohmic diffusion across the outer crust (e.g. Cumming, Zwiebel & Bildsten 2001), which will be measured in decades for all sensible values of the crustal scale height. Brown & Bildsten (1998) compute the competition between advection and ohmic diffusion for polar accretion, and find that for $\sim 0.5\dot{M}_{Edd}$ the timescale for ohmic diffusion is larger than for advection, suggesting screening may be possible on the advection timescale ($\sim 10^3 - 10^5 yr$). Recent 2D simulations (Choudhuri & Konar 2002) suggest a timescale of 10^5 years for screening by 3-4 orders of magnitude. Further work is needed to arrive at robust timescales for screening: in particular the evolution of instabilities breaking the screening (c.f. Cumming, Zweibel & Bildsten 2001) and the extension of the model to three dimensions have yet to be explored. Without information about the likely mass transfer rate of Cir X-1 immediately after the supernova, it is difficult to judge the likely effectiveness of screening, as no information is available as to the $\dot{M}$ history before the age of X-ray astronomy. The RXTE/ASM count rate and source distance suggest instantaneous accretion rates approach $\sim 3\dot{M}_{Edd}$ in the early stages of the RXTE/ASM lightcurve, while the "steady" accretion rate appears to reach $\sim 0.7\dot{M}_{Edd}$ during the "high" state (section 3). If this is an example of repeating behaviour (section 5.5), then screening of the internal magnetic field by several orders of magnitude appears at present a possibility, on a timescale ranging perhaps from 10^3 - 10^5 years. Furthermore, we remind the reader that during enhanced accretion at periastron passage, the mass transfer onto the accretor may be spherical even with strong internal B-fields. We speculate that should screening be established, this effect would further counteract outward diffusion of the internal field, as screening matter would no longer go through the stage of spreading from the poles.

6   CONCLUSION

We have examined the periodic nature of the X-ray maxima and dips exhibited in the RXTE/ASM lightcurve of Circinus X-1. We find that the X-ray dips provide a more accurate system clock than the maxima, and thus identify them with the periastron approach of the binary components. The outbursts are interpreted as the viscous timescale response of the disk to perturbations from the varying mass transfer. We attempt to use the X-ray dips to constrain the nature of the donor and the eccentricity of the orbit, and find that, within the limitations of the model used, a wider range of parameters are in principle allowed than has previously been thought, although without further exploration of the effects of nonsynchronous donor rotation, quantitative limits are at this stage unreliable. The high rate of change of the orbital period adds to the growing body of evidence that Cir X-1

is in an extremely early stage of post-supernova evolution. If the system is indeed in an early stage of post-SN evolution, the observed weak external magnetic field must suggest strong screening of the internal magnetic field of the neutron star.

7 ACKNOWLEDGEMENTS

REFERENCES

Balucinska-Church M., Church M.J., Charles P.A., Nagase F., LaSala J,. Barnard R., 2000 MNRAS 311, 861

Boyle C.B., Walker I.W., 1986 MNRAS 222, 559

Brandt W.N., Schulz N.S., 2000 ApJ Lett 544, 123

Brandt W. N., Fabian A. C., Dotani T., Nagase F., Inoue, H., Kotani T., Segawa Y., 1996 MNRAS 283, 1071

Brown J.C., Boyle C.B., 1984 A&A 141, 369 (BB84)

Brown, E.F., Bildsten L., 1998 ApJ 496, 915

Choudhuri A. R., Konar S., 2002 MNRAS 332, 933

Choudhuri A.R., *The Physics of Fluids and Plasmas*, 1st edition, 1998 CUP

Charles, P.A. et al, 1983 MNRAS 202, 657

Clark J.S., Charles P.A., Clarkson W.I., Coe M.J., 2003 A&A 400, 655

Clarkson W.I., Charles P.A., Laycock S., Coe M.J., Tout M.T., Wilson, C., 2003a MNRAS 339, 447

Clarkson W.I., Charles P.A., Laycock S., Coe M.J., 2003b MNRAS 343, 121

Clarkson W.I. & Charles P.A., 2003 MNRAS, in prep

Cumming A., Zweibel E., Bildsten L., 2001 ApJ 557, 958

Eggleton P.P., 1983 ApJ 268, 368

Fender R.P., Spencer R.,Tzioumis T., Wu K., van der Klis M., van Paradijs J., Johnston H., 1998 ApJ Lett, 506, 121

Fender, R.P., 1998 IAU Colloquium 164, eds. Zensus J.A., Taylor G.B., Wrobel J.M., astro-ph/9707317

Feng Y.X., Cui W., 2002 ApJ 564, 953

Frank J., King A.R., Raine, D.J., *Accretion Power in Astrophysics*, 3rd edition, 2002 CUP

Frank J., King A.R., Lasota J-P., 1987 A&A 178, 137 (FKL87)

Glass I.S., 1994 MNRAS 268, 742

Goss W.M., Mebold U., 1977 MNRAS 181, 255

Hanuschik R. W., Hummel W., Dietle O., Sutorius E., 1995 A&A 300, 163

Haynes R.F., Lerche I., Wright A.E., 1980 A&A 81, 83

Haynes R.F., Jauncey D.L., Murdin P.G., Goss W.M., Longmore A.J., Simons L.W.J., Milne D.K., Skellern, D.J., 1978 MNRAS 185, 661

Hughes John P., Hayashi I., Koyama, K., 1998 ApJ 505, 732

Iaria R., Burderi L., Di Salvo T., La Barbera A., Robba N.R., 2001 ApJ 547, 412

Johnston H.N., Fender R.P., Wu, K., 1999 MNRAS 308, 415

Kaluzienski L.J., Holt S.S., Boldt E.A., Serlemitsos P.J., 1976 ApJ Lett. 208, 71

van der Klis, M., 1995, in *X-ray Binaries*, eds. Lewin W.H.G., van Paradijs J., van den Heuvel P.J., first edition, CUP, p252

Konar, S., Bhattacharya D., 1997 MNRAS 284, 311

Krolik J. H., McKee C. F., Tarter C. B., 1981 ApJ 249, 422

Kuulkers, E., Wijnands, R., Belloni T., Mendez M., van der Klis M., van Paradijs J., 1998 ApJ 494, 753

Leahy D.A., 2002 A&A Lett 391, 219

Levine, A. M., Bradt, H. V., Enevoldsen, A., Morgan, E. H., Remillard, R. A., Wen, L., Smith, D. A., 2000 HEAD #32, #43.07

Levine A. M., Bradt H., Cui W., Jernigan J. G., Morgan E. H.,.; Remillard R., Shirey R. E., Smith, D. A., 1996 ApJ Lett 469, 133

Lubow S.H & Shu F.H., 1975 ApJ 198, 383

Margon B., Lampton M., Bowyer S., Cruddace R., 1971 ApJ Lett 169, 23

Marietta E., Burrows A., Fryxell B., 2000 ApJS 128, 615

Mirabel I.F., Rodriguez L.F., 1999 ARA&A 37, 409

Mignani R.P., De Luca A., Caraveo P.A., Mirabel I.F., 2002 A&A 386, 487

Moneti A., 1992 A&A Lett. 260, 7

Negueruela I., Okazaki A. T., Fabregat J., Coe M. J., Munari U., Tomov T., 2001 A&A 369, 117 (N01)

Negueruela I., Roche P., Fabregat J., Coe M. J., 1999 MNRAS 307, 695

Okazaki, A., 2001 PASJ 53, 119

Petterson J., 1978 ApJ 224, 625

Podsiadlowski Ph., 2003 MNRAS in press, astro-ph/0303660

Podsiadlowski. Ph., 1996 MNRAS 279, 1104

Romani R.W., 1990 Nature 347, 741

Saz Parkinson P.M et al., 2003 astro-ph/0303402 (SP03)

Scargle J.D., 1989 ApJ 343, 874

Scargle J.D., 1982 ApJ 263, 835

Schulz N.S., Brandt W.N., 2002 ApJ 572, 971

Shirey R.E., Bradt, H.V., Levine, A.M., 1999 ApJ 517, 472

Shirey R.E., Levine, A.M., Bradt H.V., 1999 ApJ 524, 1048

Shirey R.E., Bradt, H.V., Levine, A.M., Morgan, E.H., 1998 ApJ 506, 374

Shirey R.E., 1998 PhD Thesis, MIT

Stewart R.T., Caswell J.L., Haynes R.F., Nelson G.J., 1993 MNRAS 261, 593

Stewart R.T., Nelson G.J., Pennix W., Kitamoto S., Miyamoto S., Nicolson G.D., 1991 MNRAS 253, 212

Taam R. E., van de Heuvel E. P. J., 1986 ApJ 305, 235

Tanaka, Y., Lewin, W.H.G., 1995, in *X-ray Binaries*, eds. Lewin W.H.G., van Paradijs J., van den Heuvel P.J., first edition, CUP, p126

Tauris & van den Heuvel 2003, astro-ph/0303456, to appear in *Compact Stellar X-ray Sources*, eds. Lewin W.H.G & van der Klis, M., CUP

Tauris T.M., Fender R.P., van den Heuvel E.P.H., Johnston H.M., Wu K., MNRAS 1999, 310, 1165

van Teeseling A. & King A.R., 1998 A&A 338, 957

Tennant A.F., 1987 MNRAS 226, 971

Tennant A.F., Fabian A.C. & Shafer R.A., 1986a MNRAS 221P, 27

Tennant A.F., Fabian A.C. & Shafer R.A., 1986b MNRAS 219, 87

Warner 1995, *Cataclysmic Variables*, first edition, 1995, CUP

Whelan 1977, J.A.J. et al., MNRAS 181, 259

Zahn, J-P., 1977 A&A 57, 383